Neurochemistry International 124 (2019) 256–263

Contents lists available at ScienceDirect

Neurochemistry International

journal homepage: www.elsevier.com/locate/neuint

Extracellular adenosine and slow-wave sleep are increased after ablation of nucleus accumbens core astrocytes and neurons in mice

Xuzhao Zhou[a,b], Yo Oishi[a], Yoan Cherasse[a], Mustafa Korkutata[a,c], Shinya Fujii[a,b], Chia-Ying Lee[a,c], Michael Lazarus[a,*]

[a] International Institute for Integrative Sleep Medicine (WPI-IIIS), University of Tsukuba, Tsukuba, Ibaraki, 305-8575, Japan
[b] Doctoral Program of Biomedical Sciences, Graduate School of Comprehensive Human Sciences, University of Tsukuba, Tsukuba, Ibaraki, 305-8575, Japan
[c] PhD Program in Human Biology, School of Integrative and Global Majors, University of Tsukuba, Tsukuba, Ibaraki, 305-0005, Japan

ARTICLE INFO

Keywords:
Nucleus accumbens
Astrocytes
Diphtheria toxin
Microglia
Slow-wave sleep
Adenosine A_{2A} receptor

ABSTRACT

Sleep and wakefulness are controlled by a wide range of neuronal populations in the mammalian brain. Activation of adenosine A_{2A} receptor (A_{2A}R)-expressing neurons in the nucleus accumbens (NAc) core promotes slow-wave sleep (SWS). The neuronal mechanism by which activation of NAc A_{2A}R neurons induces SWS, however, is unknown. We hypothesized that the ability of NAc activation to induce sleep is mediated by the classic somnogen adenosine, which can be formed by various processes in all types of cells. Here, to investigate whether astrocytes are involved in the ability of the NAc to regulate SWS, we ablated glial fibrillary acidic protein (GFAP)-positive cells in the NAc core of mice by virus-mediated expression of diphtheria toxin (DT) receptors and intraperitoneal administration of DT. Analysis of electroencephalogram and electromyogram recordings of DT-treated wild-type mice revealed that SWS was remarkably increased at 1 week after DT treatment, whereas sleep-wake behavior was unchanged in DT-treated A_{2A}R knockout mice. Cell ablation was associated with an increased number of GFAP-positive cells and activation of microglia in the NAc. *In-vivo* microdialysis revealed significantly increased levels of extracellular adenosine in the NAc at 1 week after DT treatment. Our findings suggest that elevated adenosine levels in the NAc core promote SWS by acting on A_{2A}Rs and provide the first evidence that adenosine is an endogenous candidate for activating NAc A_{2A}R neurons that have the ability to induce SWS.

1. Introduction

Sleep is a common phenomenon in organisms ranging from simple worms to human beings, but is still poorly understood. Adenosine A_{2A} receptor (A_{2A}R)-expressing neurons in the nucleus accumbens (NAc) play a prominent role in sleep control mediated by motivated behavior (Oishi et al., 2017). Adenosine is an obvious candidate molecule that activates NAc A_{2A}R-expressing neurons because sufficient levels of adenosine, a well-described endogenous somnogen (Porkka-Heiskanen et al., 1997), are available under basal conditions and excitatory A_{2A}Rs are abundantly expressed in the indirect pathway of the NAc (Rosin et al., 1998). The source of the adenosine, however, remains obscure.

In principle, adenosine (and ATP, which is rapidly degraded into adenosine) can be released in the brain from neurons and glia cells. Genetically engineered mice in which a dominant negative soluble N-ethylmaleimide-sensitive factor attachment protein receptor (dnSNARE) domain is selectively expressed in astrocytes to non-specifically block the release of ATP exhibit decreased levels of extracellular adenosine and recovery sleep after sleep deprivation (Chen and Scheller, 2001; Halassa et al., 2009; Pascual et al., 2005; Raingo et al., 2012), suggesting that adenosine released from astrocytes is involved in the accumulation of sleep pressure. Moreover, adenosinergic regulation of the homeostatic sleep need via activation of neuronal adenosine A_1 receptors is controlled by glial adenosine kinase (Bjorness et al., 2016). These findings implicate astrocytes as a promising source of adenosine in sleep regulation; however, the role of NAc astrocytes in sleep regulation is not known.

In this study, we ablated some glial fibrillary acidic protein (GFAP)-positive cells, likely astrocytes, and a small number of neurons in the NAc of mice using virus-mediated expression of diphtheria toxin (DT) receptors (DTR) and intraperitoneal (i.p.) administration of DT. Extracellular adenosine and slow-wave sleep (SWS) were both increased in A_{2A}R wild-type mice, but SWS was not increased in A_{2A}R knockout mice. Surprisingly, the ablation led to an increased number of

* Corresponding author. International Institute for Integrative Sleep Medicine, University of Tsukuba, 1-1-1 Tennodai, Tsukuba, Ibaraki, 305-8575, Japan.
E-mail address: lazarus.michael.ka@u.tsukuba.ac.jp (M. Lazarus).

https://doi.org/10.1016/j.neuint.2019.01.020
Received 29 October 2018; Received in revised form 7 January 2019; Accepted 19 January 2019
Available online 25 January 2019
0197-0186/

GFAP-positive cells and activated microglia in the NAc.

2. Materials & methods

2.1. Animals

A mouse strain expressing enhanced yellow fluorescent protein (EYFP) in mouse GFAP-positive cells (lox-stop-lox-EYFP/mGFAP-Cre) was established by crossing R26-stop-EYFP mice (Jackson Laboratory, strain number 007903) (Srinivas et al., 2001) with mGFAP-Cre mice (Garcia et al., 2004). In addition, a global $A_{2A}R$ knockout mouse line was used (Chen et al., 1999). All mice (weighing 20–35 g, 8–24 weeks old) used in the present study were housed at a constant temperature of 23 ± 1 °C with a relative humidity of 60 ± 2% on an automatically controlled 12-h light/dark cycle (lights on at 7:00, off at 19:00), and provided water and food ad libitum. All experiments were performed in accordance with the Animal Care Committee of the University of Tsukuba and the National Institutes of Health Guide for the Care and Use of Laboratory Animals, and every effort was made to minimize the number of animals used, as well as any pain and discomfort.

2.2. Plasmids and adeno-associated virus (AAV) generation

To generate the pAAV-GFAP-DTR-P2A-mCherry plasmid, the hM4D (Gi) fragment in pAAV-GFAP-hM4D(Gi)-mCherry, kindly provided by Dr. Bryan Roth (University of North Carolina; Addgene plasmid #50479), was replaced with a polymerase chain reaction (PCR)-amplified fragment containing the DTR-P2A coding sequence using restriction cloning.

The AAV serotypes of shH10 for recombinant AAV-GFAP-DTR-mCherry and AAV-GFAP-mCherry were generated as described previously (Zolotukhin et al., 1999). In brief, the AAVs were generated by tripartite transfection into 293A cells. After 3 days, the 293A cells were resuspended in artificial cerebrospinal fluid, freeze-thawed four times, and treated with Benzonase® nuclease (Millipore, Burlington, MA) to degrade all forms of DNA and RNA. Subsequently, the cell debris was removed by centrifugation and the virus titer in the supernatant was determined using an AAVpro Titration Kit for Real Time PCR (Takara Bio, Kusatsu, Japan).

2.3. Stereotaxic AAV injection, electroencephalogram (EEG)/electromyogram (EMG) recordings and vigilance state assessment

Surgeries for brain microinjections were conducted under pentobarbital anesthesia (60 mg/kg, i.p.). Using aseptic techniques, the mice were stereotaxically and bilaterally injected into the NAc with recombinant AAV-GFAP-DTR-mCherry (264 nl/side, 1×10^{11} particles ml^{-1}) or AAV-GFAP-mCherry (264 nl/side, 9×10^{10} particles ml^{-1}) with a glass micropipette and an air pressure injector system (Chamberlin et al., 1998). The following coordinates were used according to the mouse brain atlas of Paxinos and Franklin (2001): AP + 1.5 mm; ML ± 1.2 mm; DV –4.1 mm.

Mice were chronically implanted with EEG and EMG electrodes for polysomnography, as previously described (Oishi et al., 2016). Briefly, the implant contained two stainless-steel screws (1 mm diameter) serving as EEG electrodes, one of which was placed epidurally over the right frontal cortex (1.0 mm anterior and 1.5 mm lateral to bregma) and the other over the right parietal cortex (1.0 mm anterior and 1.5 mm lateral to lambda). Two insulated Teflon-coated, silver wires (0.2 mm in diameter), which were placed bilaterally into the trapezius muscles, served as EMG electrodes. Both EEG and EMG electrodes were connected to a microconnector, and the whole assembly was then fixed to the skull with self-curing dental acrylic resin.

After recovering for at least 3 weeks, the mice were connected to an EEG/EMG recording cable in a soundproof recording chamber and habituated for at least 3 days before any polysomnographic recording. The EEG/EMG signals were amplified, filtered (EEG, 0.5–30 Hz; EMG, 20–200 Hz), digitized at a sampling rate of 128 Hz, and recorded using SLEEPSIGN software ver. 3 (Kissei Comtec, Matsumoto, Japan) (Kohtoh et al., 2008).

EEG/EMG data visualized by the analysis software were calculated in 10-s epochs and three stages were recognized based on their spectrum and wave properties (Oishi et al., 2016): SWS, rapid eye movement (REM) sleep, and wakefulness. Percent change of slow-wave activity (SWA) was calculated based on the SWS delta power (0.5–4 Hz) during 24 h and normalized to the baseline condition.

2.4. Microdialysis in freely behaving mice and measurement of adenosine by high-performance liquid chromatography (HPLC)

Under pentobarbital anesthesia (60 mg/kg, i.p.), mice were bilaterally implanted with guide cannulas (inner diameter 0.40 mm, outer diameter 0.50 mm; Eicom, Kyoto, Japan) into the brain using the following coordinates according to the mouse brain atlas of Paxinos and Franklin (2001): AP +1.4 mm; ML ± 1.2 mm; DV −2.9 mm. Two stainless-steel screws (1 mm diameter) were also implanted to stabilize the guide cannulas, and then dummy cannulas (diameter 0.37 mm, Eicom) were inserted to prevent the guide cannula from clogging. After recovering for at least 3 weeks, the mice were transferred to the recording chambers for habituation. On the sampling day, each mouse was quickly anesthetized using isoflurane and the dummy cannula was removed followed by insertion of the microdialysis probe (1 mm membrane length, 8.4% adenosine recovery rate; Eicom) into the guide cannula. The probe was infused continuously using an infusion pump with Ringer's solution (147 mM NaCl, 4 mM KCl, and 2.4 mM $CaCl_2$) at a flow rate of 0.5 µl/min. Two hours after inserting the probe, dialysates were continuously collected from the probe for 3 h. The dialysates were kept at −20 °C until adenosine was measured by HPLC. A TSKgel®ODS-100V HPLC column (Tosoh Bioscience, Tokyo, Japan) together with a mobile phase comprising 100 mM NaH_2PO_4 and acetonitrile in a ratio of 96:4 at a flow rate of 1 ml/min was used for HPLC separation, and 80 µl of each dialysate was injected into a HPLC-LabSolutions LC system (Shimadzu, Kyoto, Japan) equipped with a UV (260 nm) detection system. External adenosine standards were used to determine the retention time and to calculate the adenosine concentrations in the dialysates by the HPLC software.

2.5. Histology

Under deep chloral hydrate (500 mg/kg, i.p.) anesthesia, the mice were perfused via the heart with saline followed by a 10% formalin solution. The brains were removed and immersed in the same fixative overnight at 4 °C and then transferred into a 20% sucrose solution.

For immunohistochemistry, the brains were then frozen on dry ice and sectioned at 40 µm on a freezing microtome (Thermo Fisher Scientific, Waltham, MA). Immunohistochemistry was performed on free-floating sections as described previously (Lazarus et al., 2011). In brief, the sections were rinsed in PBS, incubated in 0.3% hydrogen peroxide in PBS for 30 min at room temperature, and then sequentially incubated at room temperature in 3% normal donkey serum and 0.25% Triton X-100 in PBS (PBT) for 1 h and then overnight in primary antibody diluted in PBT with 0.02% sodium azide. After overnight incubation with rabbit anti-DsRed antibody (1:5000; Cat# 632496, Takara Bio), the sections were rinsed and incubated for 2 h in biotinylated antibody (Jackson ImmunoResearch Lab, West Grove, PA) at a dilution of 1:1000. All tissue sections were then treated with avidin-biotin complex (1:1000; Vectastain ABC Elite kit, Vector Labs, Burlingame, CA) for 1 h, and immunoreactive cells were visualized by reaction with 3,3′-diaminobenzidine and 0.01% hydrogen peroxide. Tissue sections mounted on glass slides were scanned with a Hamamatsu NanoZoomer-XR Digital slide scanner (Hamamatsu Photonics, Hamamatsu, Japan), and digital photomicrographs were analyzed using Hamamatsu

NDPView software v2.4.26.

For fluorescent double-labeling, the sections were rinsed in PBT and incubated in PBT containing 10% BlockAce (DS PharmaBiomedical, Osaka, Japan) for 30 min at room temperature. The sections were then incubated with the rabbit anti-GFAP antibody (1:200, Cat# HPA056030, Sigma-Aldrich, St. Louis, MO), goat anti-mCherry antibody (1:1000, Cat# AB0040-200, SICGEN, Cantanhede, Portugal), mouse anti-NeuN antibody (1:100, Cat# MAB377, Millipore), rabbit anti-S100β (1:100, Cat# HPA015768, Sigma-Aldrich, St. Louis, MO) or rabbit anti-TMEM119 antibody (1:200, Cat# ab209064, Abcam, Cambridge, UK) containing 5% BlockAce at room temperature in the combinations described in the Results section. After overnight incubation, the sections were rinsed in PBT and incubated with donkey anti-goat Alexa Fluor® 594 nm (1:1000, Thermo Fisher Scientific), donkey anti-mouse Alexa Fluor® 647 nm (1:500, Thermo Fisher Scientific), or donkey anti-rabbit Alexa Fluor® 647 nm (1:500, Thermo Fisher Scientific) containing 5% BlockAce for at least 2 h. The sections were then mounted on glass slides and sealed with mounting medium containing DAPI dye (Vector Labs, Cat# H-1200) and cover glass. Fluorescence signals were visualized using an LSM 700 confocal microscope (Zeiss, Oberkochen, Germany).

For quantitative histologic analysis, pictures of tissues containing the NAc at the same bregma level were obtained using a confocal microscope in the Z stack mode. In Fig. 1b, a 0.35 mm × 0.35 mm area in the NAc of each tissue was analyzed. The percentage of NeuN/mCherry and S100β/mCherry-positive cells among mCherry/DAPI-positive cells was calculated. In Fig. 3g, the number of GFAP/DAPI-positive cells was counted in and normalized to the AAV area. The AAV area (i.e., the area showing mCherry expression) was measured using ImageJ software.

2.6. Statistical analysis

Data are presented as mean ± standard error of the mean (SEM) and were analyzed using SPSS statistics 25 (IBM, Armonk, NY). One-way analysis of variances (ANOVA) followed by the Fisher's Protected Least Significant Difference (PLSD) test or two-way ANOVA followed by the PLSD test was performed for all the statistical analysis. In all cases, a p-value less than 0.05 was considered significant.

3. Results

3.1. SWS increased after cytotoxic ablation of NAc GFAP-positive cells

To examine the role of NAc astrocytes in sleep–wake regulation, we ablated GFAP-positive cells in the NAc core of mice by stereotaxic microinjection of AAV carrying DTR under a GFAP promoter (AAV-GFAP-DTR, Fig. 1a) and i.p. injection of DT (Wako, Japan) 3 weeks after microinjection (Saito et al., 2001). AAV-GFAP-DTR was injected in lox-stop-lox-EYFP/mGFAP-Cre mice, denoted as $A_{2A}R^{WT}$ mice, or $A_{2A}R$ knockout mice ($A_{2A}R^{KO}$ mice).

First, we evaluated the specificity of DTR expression in AAV-GFAP-DTR-injected $A_{2A}R^{WT}$ mice by immunohistochemical investigation of the expression of the neuronal marker NeuN, the astrocytic marker S100β and the AAV-reporter protein mCherry (Fig. 1b). We detected 21.4% ± 3.5% of NeuN/mCherry-positive cells and 73.0% ± 5.8% of S100β/mCherry-positive cells among all mCherry-positive cells across six NAc-containing brain sections from three mice in each group, suggesting that most infected cells were astrocytes but a minority were neurons.

Next, we stereotaxically microinjected AAV-GFAP-DTR bilaterally into the NAc core of $A_{2A}R^{WT}$ mice, denoted as $A_{2A}R^{WT}$ NAc GFAP-DTR mice, and as controls, we injected AAV-GFAP-mCherry into the NAc core of $A_{2A}R^{WT}$ mice ($A_{2A}R^{WT}$ NAc GFAP-mCherry mice; Fig. 2a and b). Three weeks after the AAV injections, EEG and EMG recordings of the mice were analyzed to assess the baseline sleep/wake behavior of the animals. Initially, only $A_{2A}R^{WT}$ NAc GFAP-DTR mice were treated with DT (50 μg/kg, i.p.), and EEG and EMG recordings were obtained on days 9–14 following the treatment. We analyzed SWS amounts in $A_{2A}R^{WT}$ NAc GFAP-DTR mice during dark and light periods compared with the baseline. We found that SWS was significantly increased in the dark and light periods of day 9 and then gradually returned to the baseline level until day 14 (Fig. 2c). Therefore, we next obtained EEG

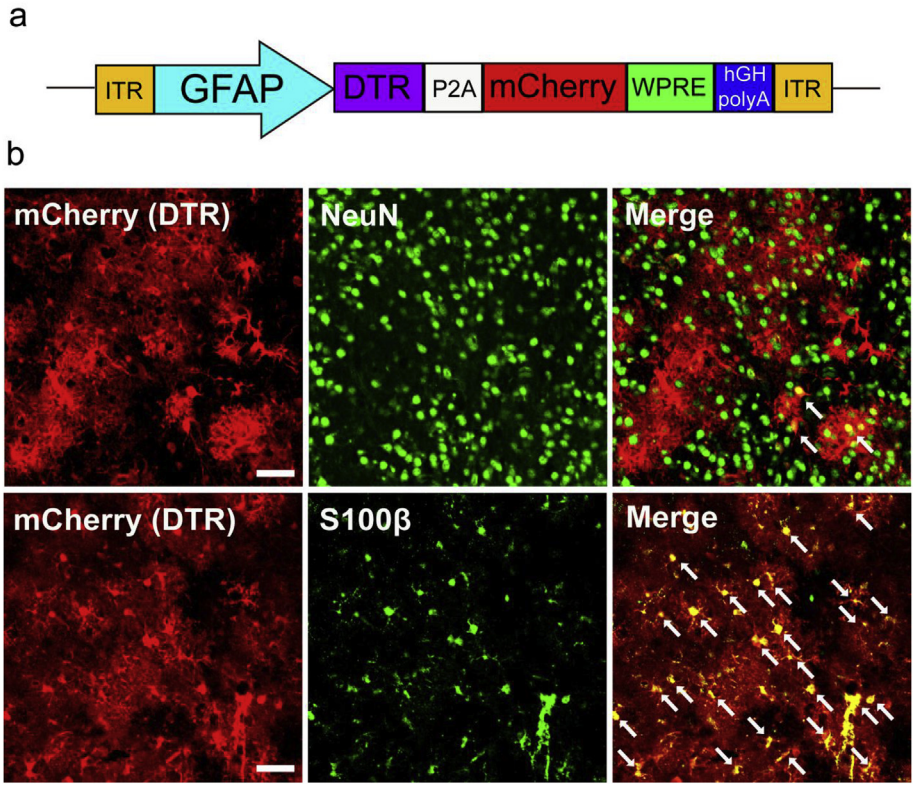

Fig. 1. Adeno-associated virus-mediated expression of diphtheria toxin receptors (DTR). **a** Construct for multi-gene expression of DTR and mCherry via 2A self-cleaving peptide driven by the glial fibrillary acidic protein (GFAP)-promoter. Other abbreviations: ITR, inverted terminal repeat sequence; P2A, 2A self-cleaving peptide; WPRE, woodchuck hepatitis virus post-transcriptional regulatory element; hGH poly A, human growth hormone polyadenylation site. **b** DTR is expressed in astrocytes and a small number of neurons after AAV infection as revealed by immunohistochemical staining with antibodies against the neuronal marker NeuN, astrocytic marker S100β and AAV reporter protein mCherry. White arrows indicate NeuN/mCherry-positive (top right panel) or S100β/mCherry-positive (bottom right panel) cells. Scale bar: 40 μm.

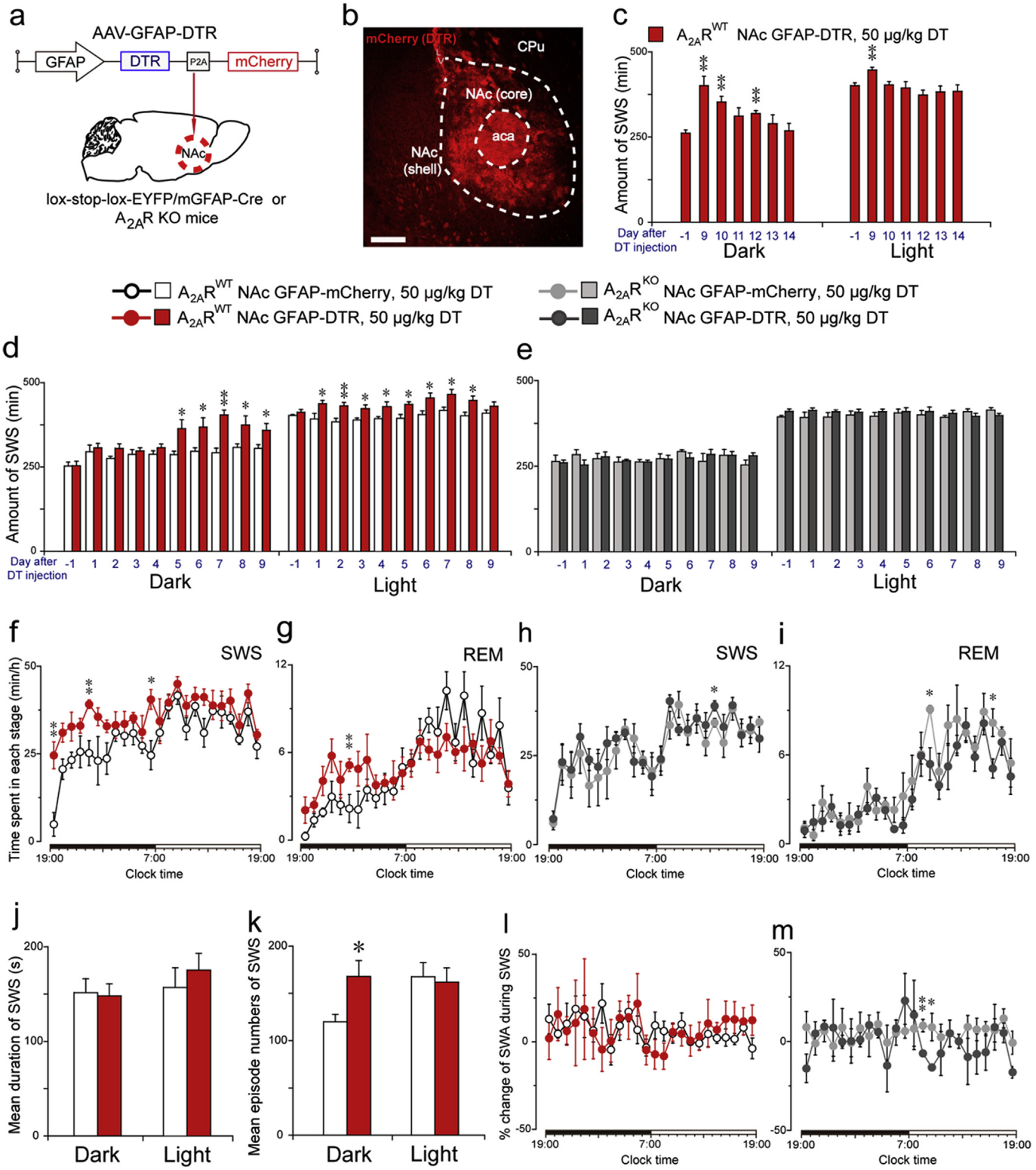

Fig. 2. SWS is increased after cytotoxic ablation of GFAP-positive cells in the NAc core in $A_{2A}R^{WT}$ but not in $A_{2A}R^{KO}$ NAc GFAP-DTR mice. **a** AAV-GFAP-DTR was bilaterally microinjected into lox-stop-lox-EYFP/mGFAP-Cre ($A_{2A}R^{WT}$) or $A_{2A}R^{KO}$ mice. **b** Typical AAV infection in the NAc core as indicated by mCherry expression. Abbreviations used: aca, anterior commissure; CPu, caudate putamen. Scale bar: 200 μm **c** SWS during the dark and light periods 1 day before and at 9–14 days after DT treatment in $A_{2A}R^{WT}$ NAc GFAP-DTR mice ($n = 4$). $^{**}p < 0.01$ vs baseline day (i.e., day before DT treatment), assessed by one-way ANOVA. **d** SWS during the dark and light periods 1 day before and for 9 days after DT treatment in $A_{2A}R^{WT}$ NAc GFAP-mCherry ($n = 5$) and NAc GFAP-DTR ($n = 6$) mice. $^{*}p < 0.05$, $^{**}p < 0.01$ vs $A_{2A}R^{WT}$ NAc GFAP-mCherry mice; assessed by one-way ANOVA. **e** SWS during the dark and light periods 1 day before and at 1–9 days after DT treatment in $A_{2A}R^{KO}$ NAc GFAP-mCherry ($n = 4$) and NAc GFAP-DTR ($n = 6$) mice. **f-i** SWS (**f, h**), and REM-sleep (**g, i**) time-courses of all the mouse groups on day 7 after DT treatment. $^{*}p < 0.05$, $^{**}p < 0.01$ vs $A_{2A}R^{WT}$ NAc GFAP-mCherry (**f, g**) or $A_{2A}R^{KO}$ NAc GFAP-mCherry (**h, i**) mice; assessed by two-way ANOVA followed by the PLSD test. **j, k** Mean duration (**j**) and number (**k**) of SWS episodes during the dark and light periods on day 7 after DT treatment in $A_{2A}R^{WT}$ NAc GFAP-mCherry ($n = 5$) and $A_{2A}R^{WT}$ NAc GFAP-DTR ($n = 6$) mice. $^{*}p < 0.05$ vs $A_{2A}R^{WT}$ NAc GFAP-mCherry mice, assessed by one-way ANOVA. **l, m** SWS-SWA time-courses of all the mouse groups on day 7 after DT treatment. $^{*}p < 0.05$, $^{**}p < 0.01$ vs $A_{2A}R^{KO}$ NAc GFAP-mCherry mice; assessed by two-way ANOVA followed by the PLSD test.

and EMG recordings of $A_{2A}R^{WT}$ NAc GFAP-DTR and NAc GFAP-mCherry mice for 9 days after DT treatment. SWS increased in the $A_{2A}R^{WT}$ NAc GFAP-DTR mice during the dark period from day 5 after DT treatment before reaching a maximum on day 7 after DT treatment, compared with DT-treated control mice (day 5: $F_{(1, 9)} = 7.808$, $p = 0.011$; day 6: $F_{(1, 9)} = 6.470$, $p = 0.024$; day 7: $F_{(1, 9)} = 21.858$, $p = 0.0001$; day 8: $F_{(1, 9)} = 6.907$, $p = 0.026$; day 9: $F_{(1, 9)} = 8.050$, $p = 0.023$; Fig. 2d). SWS also increased significantly in the $A_{2A}R^{WT}$ NAc GFAP-DTR mice during the light period between days 1 and 8, compared to the DT-treated control mice (day 1: $F_{(1, 9)} = 3.948$, $p = 0.015$; day 2: $F_{(1, 9)} = 7.591$, $p = 0.002$; day 3: $F_{(1, 9)} = 3.205$, $p = 0.024$; day 4: $F_{(1, 9)} = 2.971$, $p = 0.031$; day 5: $F_{(1, 9)} = 4.316$, $p = 0.012$; day 6: $F_{(1, 9)} = 4.379$, $p = 0.021$; day 7: $F_{(1, 9)} = 8.384$, $p = 0.011$; day 8: $F_{(1, 9)} = 6.679$, $p = 0.013$; Fig. 2d). We also stereotaxically microinjected AAV-GFAP-DTR bilaterally into the NAc core of $A_{2A}R^{KO}$ mice, denoted as $A_{2A}R^{KO}$ NAc GFAP-DTR mice, and as controls, we injected AAV-GFAP-mCherry into the NAc core of $A_{2A}R^{KO}$ mice ($A_{2A}R^{KO}$ NAc GFAP-mCherry mice; Fig. 2a). SWS was not increased in DT-treated $A_{2A}R^{KO}$ NAc GFAP-DTR mice, however, compared with $A_{2A}R^{KO}$ NAc GFAP-mCherry mice in either the dark or light periods (Fig. 2e). This observation suggests that the SWS increase after DT treatment is mediated by adenosine via $A_{2A}R$.

On day 7, when the mice had the strongest SWS increase, $A_{2A}R^{WT}$ NAc GFAP-DTR mice exhibited increased SWS and REM sleep, especially during the dark period, compared with DT-treated control mice (Fig. 2f and g). Concomitantly, $A_{2A}R^{WT}$ NAc GFAP-DTR mice had a lower amount of wakefulness (data not shown). By contrast, we did not observe notable changes in the hourly SWS and REM sleep amounts of $A_{2A}R^{KO}$ NAc GFAP-DTR mice on day 7 after DT treatment, compared with $A_{2A}R^{KO}$ NAc GFAP-mCherry mice (Fig. 2h and i). The increased amount of SWS in $A_{2A}R^{WT}$ NAc GFAP-DTR mice during the dark period of day 7 after DT treatment was due to an increased number of SWS episodes, while the mean duration of SWS episodes was not changed (Fig. 2j and k).

A change in SWA is considered a hallmark of sleep homeostasis disturbance (Dispersyn et al., 2017; Wang et al., 2018). To investigate whether sleep homeostasis was affected by cytotoxic ablation of NAc GFAP-positive cells, we calculated changes in SWA on day 7 normalized to the baseline; however, there was no significant difference in the normalized SWA in all the mouse groups (Fig. 2l, m).

3.2. Cytotoxic ablation of NAc GFAP-positive cells led to increased activation of astrocytes and microglia

We then evaluated the effects of cytotoxic ablation of GFAP-positive cells in the NAc after DT treatment by immunohistochemical investigation of the expression of the astrocyte-reporter protein EYFP and the AAV-reporter protein mCherry (Fig. 3a–c). No EYFP- and mCherry-positive cells were observed in $A_{2A}R^{WT}$ NAc GFAP-DTR mice after DT treatment (Fig. 3a), whereas many double-positive cells were observed in $A_{2A}R^{WT}$ NAc GFAP-DTR mice treated with saline or $A_{2A}R^{WT}$ NAc GFAP-mCherry mice treated with DT (Fig. 3b and c). These findings suggest that cells infected with AAV-GFAP-DTR were completely ablated by the administration of DT.

Next, we examined the residual NAc astrocytes on day 7 after DT administration by immunohistochemical investigation of the expression of the endogenous astrocyte marker GFAP and the AAV-reporter protein mCherry (Fig. 3d–f). Surprisingly, GFAP expression was remarkably increased in $A_{2A}R^{WT}$ NAc GFAP-DTR mice treated with DT compared with $A_{2A}R^{WT}$ NAc GFAP-DTR mice treated with saline or $A_{2A}R^{WT}$ NAc GFAP-mCherry mice treated with DT. The number of GFAP-expressing cells within the AAV infection area, as indicated by the mCherry expression, was significantly higher than that in the control mice ($F_{(2, 14)} = 10.380$, $p = 0.008$, $A_{2A}R^{WT}$ NAc GFAP-DTR/DT *vs* $A_{2A}R^{WT}$ NAc GFAP-DTR/saline; $F_{(2, 14)} = 10.380$, $p = 0.001$, $A_{2A}R^{WT}$ NAc GFAP-DTR/DT *vs* $A_{2A}R^{WT}$ NAc GFAP-mCherry/DT, Fig. 3g).

Because we observed an unexpected increase in GFAP expression after cytotoxic ablation of NAc GFAP-positive cells, we also examined the morphology of microglia in $A_{2A}R^{WT}$ NAc GFAP-DTR mice by immunohistochemical analysis with an antibody against the microglia marker TMEM119 (Fig. 3h and i). Activated microglia were detected in DT-treated $A_{2A}R^{WT}$ NAc GFAP-DTR mice (Fig. 3i), but not in DT-treated $A_{2A}R^{WT}$ NAc GFAP-mCherry mice. This observation suggests DT-mediated apoptosis of GFAP cells in the NAc is accompanied by microglia activation.

3.3. Extracellular adenosine levels increased after ablation of NAc GFAP-positive cells

Finally, we investigated extracellular adenosine levels on day 7 after DT treatment using microdialysis (Fig. 4a and b). The dialysates were collected between 19:00 and 22:00 when there is a large increase in SWS and analyzed by HPLC. Dialysates were collected before and after DT treatment by inserting the same probe in contralateral sites of the mouse brain. The adenosine concentration was determined by comparison with adenosine standards (Fig. 4c) and normalized between the samples taken before and after DT treatment due to the varying recovery rates of the microdialysis probes. The position of the microdialysis probe was confirmed by immunohistochemical analysis of the expression of the AAV reporter protein mCherry (Fig. 4d).

Adenosine levels increased significantly after DT administration in $A_{2A}R^{WT}$ and $A_{2A}R^{KO}$ NAc GFAP-DTR mice, compared with $A_{2A}R^{WT}$ NAc GFAP-mCherry mice ($A_{2A}R^{WT}$ NAc GFAP-mCherry *vs* $A_{2A}R^{WT}$ NAc GFAP-DTR, $F_{(2, 10)} = 4.486$, $p = 0.037$; $A_{2A}R^{WT}$ NAc GFAP-mCherry *vs* $A_{2A}R^{KO}$ NAc GFAP-DTR, $F_{(2, 10)} = 4.486$, $p = 0.019$; Fig. 4e). These findings suggest that ablation of GFAP-positive cells in the NAc results in an increase in extracellular adenosine, at least on day 7 after cell apoptosis is initiated by DT treatment.

4. Discussion

A recent study showed that chemogenetic or optogenetic activation of NAc core $A_{2A}R$ neurons projecting to the ventral pallidum strongly induces SWS, whereas chemogenetic inhibition of these neurons prevents sleep induction, but does not affect the homoeostatic sleep rebound (Oishi et al., 2017). We hypothesized that adenosine is a candidate molecule for activating NAc $A_{2A}R$ neurons. Where in the NAc adenosine is generated, however, remains unknown. Adenosine is not a neurotransmitter or a typical neuromodulator released from neurons, because it can be formed by various processes in all cell types (Ohana et al., 2001). Cytotoxic ablation of GFAP-positive cells, which are likely astrocytes, as well as a small number of neurons in the NAc led to a transient increase in SWS over several days in mice. Further analysis of the molecular mechanisms revealed that extracellular adenosine levels increased after ablation and the SWS increase was mediated by $A_{2A}R$.

Surprisingly, the number of astrocytes in the NAc core was also increased after GFAP-positive cell ablation. The increase in the number of astrocytes may be due to astrogliosis, i.e., astrocyte migration or proliferation, after apoptotic destruction of astrocytes or neurons by DT (Aldskogius and Kozlova, 1998; Morimoto and Bonavida, 1992). We suspect that the increase in extracellular adenosine is due to the increased number of astrocytes. A role for astrocytes in sleep regulation has only recently started to emerge. Extracellular levels of adenosine and recovery sleep after sleep deprivation are reduced when the release of ATP is blocked by the transgenic expression of the dnSNARE protein in astrocytes (Chen and Scheller, 2001; Halassa et al., 2009; Pascual et al., 2005; Raingo et al., 2012) and astrocytic adenosine kinase is involved in regulating homeostatic sleep (Bjorness et al., 2016). Moreover, optogenetic stimulation of astrocytes in the posterior hypothalamus increases sleep (Pelluru et al., 2016).

The possibility that activated microglia also contribute to the elevated adenosine levels cannot be excluded. Microglia are immune cells

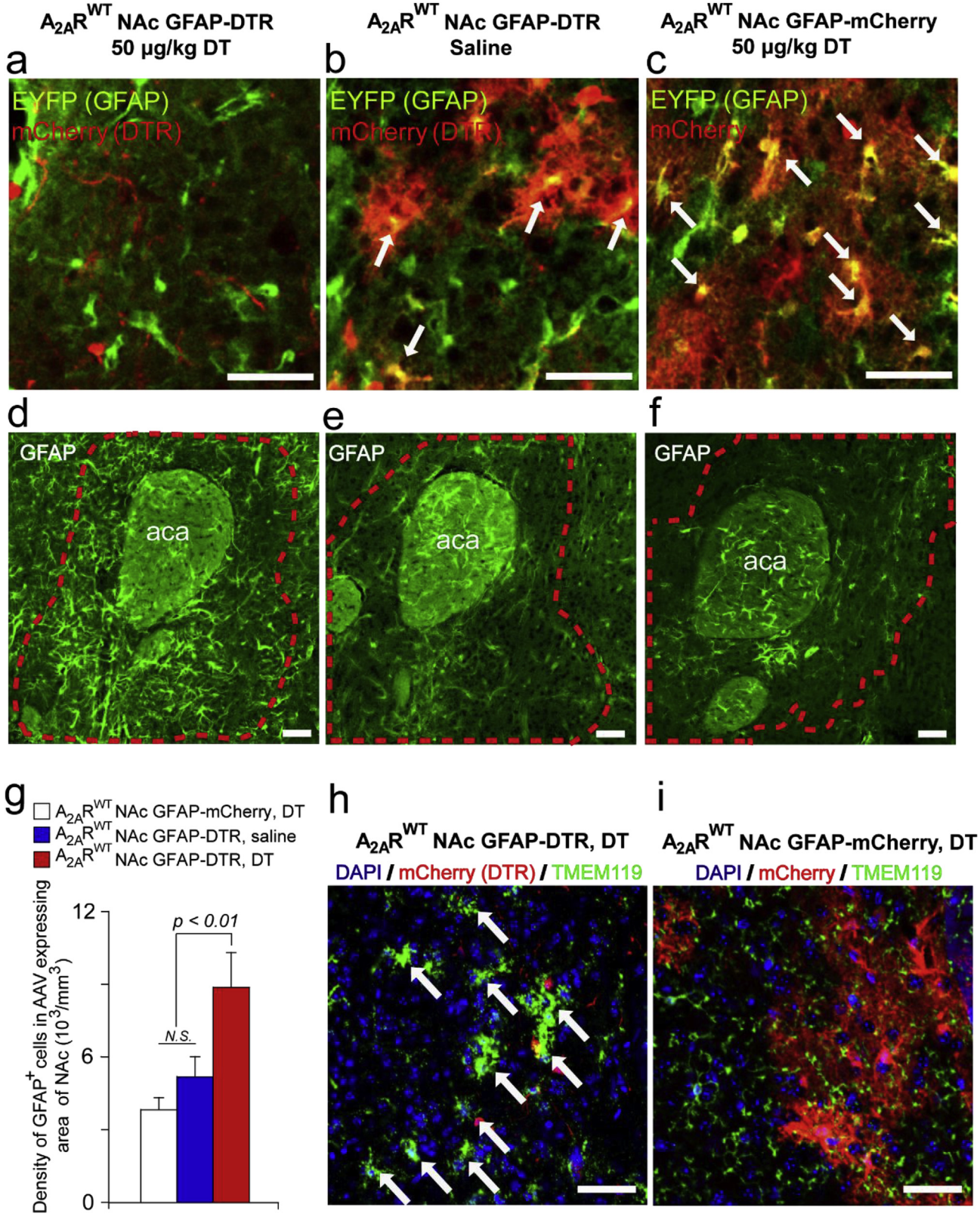

Fig. 3. The number of GFAP-expressing cells is increased and microglia are activated after cytotoxic ablation of NAc GFAP-positive cells. **a-c** AAV-infected cells are destroyed in DT-treated $A_{2A}R^{WT}$ NAc GFAP-DTR mice (**a**) but not in saline-treated $A_{2A}R^{WT}$ NAc GFAP-DTR (**b**) or DT-treated $A_{2A}R^{WT}$ NAc GFAP-mCherry mice (**c**) on day 7 after DT injection. White arrows indicate AAV-infected astrocytes. Scale bars: 50 µm. **d-f** Increased number of GFAP-positive cells in DT-treated $A_{2A}R^{WT}$ NAc GFAP-DTR (**d**) compared with saline-treated $A_{2A}R^{WT}$ NAc GFAP-DTR (**e**) or DT-treated $A_{2A}R^{WT}$ NAc GFAP-mCherry mice (**f**). Scale bars: 50 µm. Red dashed lines indicate area with mCherry expression. **g** Number of GFAP-positive cells (astrocytes) in the AAV-infected area on day 7 after DT treatment in $A_{2A}R^{WT}$ NAc GFAP-DTR/DT ($n = 6$), $A_{2A}R^{WT}$ NAc GFAP-DTR/saline ($n = 5$) and $A_{2A}R^{WT}$ NAc GFAP-mCherry/DT ($n = 6$) mice. Significance was assessed by one-way ANOVA followed by the PLSD test. **h, i** Immunostaining of activated or ramified microglia in $A_{2A}R^{WT}$ NAc GFAP-DTR (**h**) or $A_{2A}R^{WT}$ NAc GFAP-mCherry mice (**i**), respectively, after DT treatment. White arrows indicate activated/phagocytic microglia in the NAc. Scale bars: 40 µm.

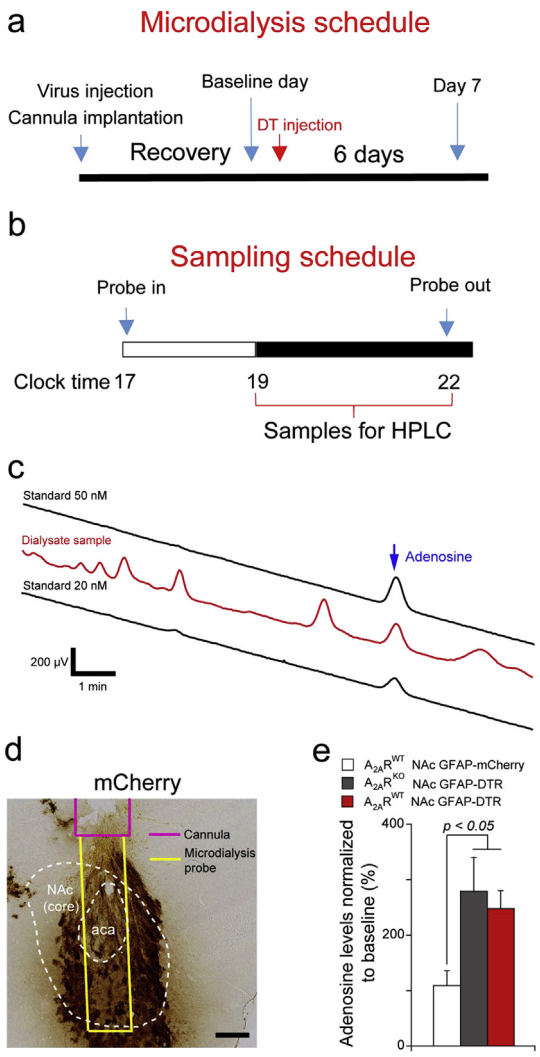

Fig. 4. Measurement of extracellular adenosine levels in the NAc by microdialysis. **a** Microdialysis schedule before and after DT treatment. **b** Sampling schedule after inserting the microdialysis probe. **c** Typical HPLC chromatograms of a dialysate and external adenosine standards. **d** Typical implantation site for the guide cannula and location of the microdialysis probe in the NAc. Immunostaining for mCherry indicates the AAV-infected area in the NAc. Scale bar: 200 µm **e** Extracellular adenosine levels normalized to baseline in the NAc of $A_{2A}R^{WT}$ NAc GFAP-mCherry (n = 4), $A_{2A}R^{WT}$ NAc GFAP-DTR (n = 5), and $A_{2A}R^{KO}$ NAc GFAP-DTR (n = 4) mice on day 7 after treatment with 50 µg/kg DT. Significance was assessed by one-way ANOVA followed by the PLSD test.

distributed throughout the brain, comprising 10%–20% of the glial population (Ginhoux et al., 2013). Microglia in a phagocytic state are usually involved in the clearance of apoptotic cells (Lian et al., 2016). The role of microglia in sleep regulation remains elusive. Some studies reported that microglia are activated after sleep deprivation (Huang et al., 2014; Wadhwa et al., 2018; Wisor et al., 2011). Microglia activation is likely a consequence of sleep loss, however, rather than the cause of sleep rebound. Microglia are considered to be a major source of cytokines, but there is almost no evidence indicating that microglia can release adenosine (Hanisch, 2002; Smith et al., 2012). In contrast, adenosine has an important role in regulating microglia via adenosine receptors (Gyoneva et al., 2009; Luongo et al., 2014; Madeira et al., 2018; Orr et al., 2009). Future studies utilizing opto- or chemogenetic systems are needed to examine the ability of microglia to release adenosine and induce sleep. Moreover, cytokines have a known role in sleep/wake regulation, but the effects of cytokines released from microglia in the NAc on sleep have never been investigated. The $A_{2A}R^{KO}$ NAc GFAP-DTR mice exhibited no increase in SWS after DTR-mediated ablation of astrocytes and neurons, suggesting that cytokines are not involved in the sleep phenotype.

Moreover, the DTR was also expressed in neurons to some extent due to leakage of the GFAP promoter used in our viral vector and thus, it is possible that we also ablated a small number of neurons by DT administration. We do not consider this directly relevant, however, because the sleep/wake behavior of $A_{2A}R^{KO}$ mice is not affected by DTR-mediated ablation of astrocytes and neurons, and cytotoxic lesions of the NAc core or shell neurons induce wakefulness (Qiu et al., 2012). Neuronal ablation, however, may contribute to activate the astrocytes and microglia (Aldskogius and Kozlova, 1998).

Cytotoxic ablation of astrocytes and neurons may mimic traumatic brain injury (TBI) which is often associated with sleep disorders. TBI patients experience high rates of insomnia (29%), hypersomnia (28%), and sleep apnea (25%) (Wickwire et al., 2016). For example, hypersomnia was observed in patients with thalamic astrogliosis and increased adenosine levels in the cerebral spinal fluid during an acute period after TBI (Hazra et al., 2014; Rowe et al., 2014; Zuzuárregui et al., 2018). An imbalance of neurotransmitters (e.g., GABA, glutamate and orexin) or increased cytokine production in the hypothalamus or brain stem after TBI, however, is believed to cause the sleep disturbance (Sandsmark et al., 2017). Although adenosine is known to play an important role in neuroprotection after TBI (Lusardi, 2009), the involvement of adenosine, especially in the NAc, in TBI-related sleep disorders remains unclear.

5. Conclusion

Activation of $A_{2A}R$ neurons in the NAc core promotes SWS sleep and elevated adenosine levels in the NAc core increase SWS by acting on $A_{2A}R$. Our findings provide the first evidence that adenosine is a strong candidate molecule for activating NAc core $A_{2A}R$ neurons to induce SWS.

Conflicts of interest

The authors declare no competing interests.

Author contributions

X.Z., Y.O., Y.C., and M.L. designed the experiments. X.Z., Y.O., S.F., M.K., Y.C., and C.L. collected and analyzed the data. X.Z. and Y.O. contributed to the mouse lines. X.Z. and M.L. wrote the paper.

Acknowledgements

We thank Ms. Saki Masuda for technical assistance. This work was supported by the Japan Society for the Promotion of Science [Grant-in-Aid for Scientific Research B (grant number 17H02215) to M.L.]; the Japan Science and Technology Agency [CREST grant (grant number JPMJCR1655) to M.L.]; the Ministry of Education, Culture, Sports, Science and Technology of Japan [Grants-in-Aid for Scientific Research on Innovative Areas “Living in Space” (grant numbers 15H05935, 15K21745, 18H04966) and “Will Dynamics” (grant number 17H06047) to M.L.]; the World Premier International Research Center Initiative (WPI) from MEXT (to Y.O., Y.C., and M.L.); and a research grant of the Astellas Foundation for Research on Metabolic Disorders (to M.L.).

References

Aldskogius, H., Kozlova, E.N., 1998. Central neuron-glial and glial-glial interactions following axon injury. Prog. Neurobiol. 55 (1), 1–26.

Bjorness, T.E., Dale, N., Mettlach, G., Sonneborn, A., Sahin, B., Fienberg, A.A., Yanagisawa, M., Bibb, J.A., Greene, R.W., 2016. An adenosine-mediated glial-neuronal circuit for homeostatic sleep. J. Neurosci. 36 (13), 3709–3721. https://doi.org/10.1523/Jneurosci.3906-15.2016.

Chamberlin, N.L., Du, B., de Lacalle, S., Saper, C.B., 1998. Recombinant adeno-associated virus vector: use for transgene expression and anterograde tract tracing in the CNS. Brain Res. 793 (1–2), 169–175.
Chen, J.F., Huang, Z., Ma, J., Zhu, J., Moratalla, R., Standaert, D., Moskowitz, M.A., Fink, J.S., Schwarzschild, M.A., 1999. A(2A) adenosine receptor deficiency attenuates brain injury induced by transient focal ischemia in mice. J. Neurosci. 19 (21), 9192–9200.
Chen, Y.A., Scheller, R.H., 2001. SNARE-mediated membrane fusion. Nat. Rev. Mol. Cell Biol. 2 (2), 98–106. https://doi.org/10.1038/35052017.
Dispersyn, G., Sauvet, F., Gomez-Merino, D., Ciret, S., Drogou, C., Leger, D., Gallopin, T., Chennaoui, M., 2017. The homeostatic and circadian sleep recovery responses after total sleep deprivation in mice. J. Sleep Res. 26 (5), 531–538. https://doi.org/10.1111/jsr.12541.
Garcia, A.D., Doan, N.B., Imura, T., Bush, T.G., Sofroniew, M.V., 2004. GFAP-expressing progenitors are the principal source of constitutive neurogenesis in adult mouse forebrain. Nat. Neurosci. 7 (11), 1233–1241. https://doi.org/10.1038/nn1340.
Ginhoux, F., Lim, S., Hoeffel, G., Low, D., Huber, T., 2013. Origin and differentiation of microglia. Front. Cell. Neurosci. 7, 45. https://doi.org/10.3389/fncel.2013.00045.
Gyoneva, S., Orr, A.G., Traynelis, S.F., 2009. Differential regulation of microglial motility by ATP/ADP and adenosine. Park. Relat. Disord. 15 (Suppl. 3), S195–S199. https://doi.org/10.1016/S1353-8020(09)70813-2.
Halassa, M.M., Florian, C., Fellin, T., Munoz, J.R., Lee, S.Y., Abel, T., Haydon, P.G., Frank, M.G., 2009. Astrocytic modulation of sleep homeostasis and cognitive consequences of sleep loss. Neuron 61 (2), 213–219. https://doi.org/10.1016/j.neuron.2008.11.024.
Hanisch, U.K., 2002. Microglia as a source and target of cytokines. Glia 40 (2), 140–155. https://doi.org/10.1002/glia.10161.
Hazra, A., Macolino, C., Elliott, M.B., Chin, J., 2014. Delayed thalamic astrocytosis and disrupted sleep-wake patterns in a preclinical model of traumatic brain injury. J. Neurosci. Res. 92 (11), 1434–1445.
Huang, C.T., Chiang, R.P., Chen, C.L., Tsai, Y.J., 2014. Sleep deprivation aggravates median nerve injury-induced neuropathic pain and enhances microglial activation by suppressing melatonin secretion. Sleep 37 (9), 1513–1523. https://doi.org/10.5665/sleep.4002.
Kohtoh, S., Taguchi, Y., Matsumoto, N., Wada, M., Huang, Z.L., Urade, Y., 2008. Algorithm for sleep scoring in experimental animals based on fast Fourier transform power spectrum analysis of the electroencephalogram. Sleep Biol. Rhythm 6 (3), 163–171. https://doi.org/10.1111/j.1479-8425.2008.00355.x.
Lazarus, M., Shen, H.Y., Cherasse, Y., Qu, W.M., Huang, Z.L., Bass, C.E., Winsky-Sommerer, R., Semba, K., Fredholm, B.B., Boison, D., Hayaishi, O., Urade, Y., Chen, J.F., 2011. Arousal effect of caffeine depends on adenosine A(2A) receptors in the shell of the nucleus accumbens. J. Neurosci. 31 (27), 10067–10075. https://doi.org/10.1523/Jneurosci.6730-10.2011.
Lian, H., Roy, E., Zheng, H., 2016. Microglial phagocytosis assay. Bio Protoc 6 (21). https://doi.org/10.21769/BioProtoc.1988.
Luongo, L., Guida, F., Imperatore, R., Napolitano, F., Gatta, L., Cristino, L., Giordano, C., Siniscalco, D., Di Marzo, V., Bellini, G., Petrelli, R., Cappellacci, L., Usiello, A., de Novellis, V., Rossi, F., Maione, S., 2014. The A1 adenosine receptor as a new player in microglia physiology. Glia 62 (1), 122–132. https://doi.org/10.1002/glia.22592.
Lusardi, T.A., 2009. Adenosine neuromodulation and traumatic brain injury. Curr. Neuropharmacol. 7 (3), 228–237. https://doi.org/10.2174/157015909789152137.
Madeira, M.H., Rashid, K., Ambrosio, A.F., Santiago, A.R., Langmann, T., 2018. Blockade of microglial adenosine A2A receptor impacts inflammatory mechanisms, reduces ARPE-19 cell dysfunction and prevents photoreceptor loss in vitro. Sci. Rep. 8 (1), 2272. https://doi.org/10.1038/s41598-018-20733-2.
Morimoto, H., Bonavida, B., 1992. Diphtheria toxin- and Pseudomonas A toxin-mediated apoptosis. ADP ribosylation of elongation factor-2 is required for DNA fragmentation and cell lysis and synergy with tumor necrosis factor-alpha. J. Immunol. 149 (6), 2089–2094.
Ohana, G., Bar-Yehuda, S., Barer, F., Fishman, P., 2001. Differential effect of adenosine on tumor and normal cell growth: focus on the A3 adenosine receptor. J. Cell. Physiol. 186 (1), 19–23. https://doi.org/10.1002/1097-4652(200101)186:1<19::AID-JCP1011>3.0.CO;2-3.
Oishi, Y., Takata, Y., Taguchi, Y., Kohtoh, S., Urade, Y., Lazarus, M., 2016. Polygraphic Recording Procedure for Measuring Sleep in Mice. JoVE 107, e53678. https://doi.org/10.3791/53678.
Oishi, Y., Xu, Q., Wang, L., Zhang, B.J., Takahashi, K., Takata, Y., Luo, Y.J., Cherasse, Y., Schiffmann, S.N., de Kerchove d'Exaerde, A., Urade, Y., Qu, W.M., Huang, Z.L., Lazarus, M., 2017. Slow-wave sleep is controlled by a subset of nucleus accumbens core neurons in mice. Nat. Commun. 8 (1), 734. https://doi.org/10.1038/s41467-017-00781-4.
Orr, A.G., Orr, A.L., Li, X.J., Gross, R.E., Traynelis, S.F., 2009. Adenosine A(2A) receptor mediates microglial process retraction. Nat. Neurosci. 12 (7), 872–878. https://doi.org/10.1038/nn.2341.
Pascual, O., Casper, K.B., Kubera, C., Zhang, J., Revilla-Sanchez, R., Sul, J.Y., Takano, H., Moss, S.J., McCarthy, K., Haydon, P.G., 2005. Astrocytic purinergic signaling coordinates synaptic networks. Science 310 (5745), 113–116. https://doi.org/10.1126/science.1116916.
Paxinos, G., Franklin, K., 2001. The Mouse Brain in Stereotaxic Coordinates, second ed. Academic Press.
Pelluru, D., Konadhode, R.R., Bhat, N.R., Shiromani, P.J., 2016. Optogenetic stimulation of astrocytes in the posterior hypothalamus increases sleep at night in C57BL/6J mice. Eur. J. Neurosci. 43 (10), 1298–1306. https://doi.org/10.1111/ejn.13074.
Porkka-Heiskanen, T., Strecker, R.E., Thakkar, M., Bjorkum, A.A., Greene, R.W., McCarley, R.W., 1997. Adenosine: a mediator of the sleep-inducing effects of prolonged wakefulness. Science 276 (5316), 1265–1268. https://doi.org/10.1126/science.276.5316.1265.
Qiu, M.H., Liu, W., Qu, W.M., Urade, Y., Lu, J., Huang, Z.L., 2012. The Role of Nucleus Accumbens Core/Shell in Sleep-Wake Regulation and their Involvement in Modafinil-Induced Arousal. PLoS One 7 (9), e45471. https://doi.org/10.1371/journal.pone.0045471.
Raingo, J., Khvotchev, M., Liu, P., Darios, F., Li, Y.C., Ramirez, D.M., Adachi, M., Lemieux, P., Toth, K., Davletov, B., Kavalali, E.T., 2012. VAMP4 directs synaptic vesicles to a pool that selectively maintains asynchronous neurotransmission. Nat. Neurosci. 15 (5), 738–745. https://doi.org/10.1038/nn.3067.
Rosin, D.L., Robeva, A., Woodard, R.L., Guyenet, P.G., Linden, J., 1998. Immunohistochemical localization of adenosine A2A receptors in the rat central nervous system. J. Comp. Neurol. 401 (2), 163–186.
Rowe, R.K., Striz, M., Bachstetter, A.D., Van Eldik, L.J., Donohue, K.D., O'Hara, B.F., Lifshitz, J., 2014. Diffuse brain injury induces acute post-traumatic sleep. PLoS One 9 (1), e82507. https://doi.org/10.1371/journal.pone.0082507.
Saito, M., Iwawaki, T., Taya, C., Yonekawa, H., Noda, M., Inui, Y., Mekada, E., Kimata, Y., Tsuru, A., Kohno, K., 2001. Diphtheria toxin receptor-mediated conditional and targeted cell ablation in transgenic mice. Nat. Biotechnol. 19 (8), 746–750. https://doi.org/10.1038/90795.
Sandsmark, D.K., Elliott, J.E., Lim, M.M., 2017. Sleep-wake disturbances after traumatic brain injury: synthesis of human and animal studies. Sleep 40 (5). https://doi.org/10.1093/sleep/zsx044.
Smith, J.A., Das, A., Ray, S.K., Banik, N.L., 2012. Role of pro-inflammatory cytokines released from microglia in neurodegenerative diseases. Brain Res. Bull. 87 (1), 10–20. https://doi.org/10.1016/j.brainresbull.2011.10.004.
Srinivas, S., Watanabe, T., Lin, C.S., William, C.M., Tanabe, Y., Jessell, T.M., Costantini, F., 2001. Cre reporter strains produced by targeted insertion of EYFP and ECFP into the ROSA26 locus. BMC Dev. Biol. 1, 4.
Wadhwa, M., Chauhan, G., Roy, K., Sahu, S., Deep, S., Jain, V., Kishore, K., Ray, K., Thakur, L., Panjwani, U., 2018. Caffeine and modafinil ameliorate the neuroinflammation and anxious behavior in rats during sleep deprivation by inhibiting the microglia activation. Front. Cell. Neurosci. 12, 49. https://doi.org/10.3389/fncel.2018.00049.
Wang, Z., Ma, J., Miyoshi, C., Li, Y., Sato, M., Ogawa, Y., Lou, T., Ma, C., Gao, X., Lee, C., Fujiyama, T., Yang, X., Zhou, S., Hotta-Hirashima, N., Klewe-Nebenius, D., Ikkyu, A., Kakizaki, M., Kanno, S., Cao, L., Takahashi, S., Peng, J., Yu, Y., Funato, H., Yanagisawa, M., Liu, Q., 2018. Quantitative phosphoproteomic analysis of the molecular substrates of sleep need. Nature 558 (7710), 435–439. https://doi.org/10.1038/s41586-018-0218-8.
Wickwire, E.M., Williams, S.G., Roth, T., Capaldi, V.F., Jaffe, M., Moline, M., Motamedi, G.K., Morgan, G.W., Mysliwiec, V., Germain, A., Pazdan, R.M., Ferziger, R., Balkin, T.J., MacDonald, M.E., Macek, T.A., Yochelson, M.R., Scharf, S.M., Lettieri, C.J., 2016. Sleep, sleep disorders, and mild traumatic brain injury. What we know and what we need to know: findings from a national working group. Neurotherapeutics 13 (2), 403–417. https://doi.org/10.1007/s13311-016-0429-3.
Wisor, J.P., Schmidt, M.A., Clegern, W.C., 2011. Evidence for neuroinflammatory and microglial changes in the cerebral response to sleep loss. Sleep 34 (3), 261–272.
Zolotukhin, S., Byrne, B.J., Mason, E., Zolotukhin, I., Potter, M., Chesnut, K., Summerford, C., Samulski, R.J., Muzyczka, N., 1999. Recombinant adeno-associated virus purification using novel methods improves infectious titer and yield. Gene Ther. 6 (6), 973–985. https://doi.org/10.1038/sj.gt.3300938.
Zuzuárregui, J.R.P., Bickart, K., Kutscher, S.J., 2018. A review of sleep disturbances following traumatic brain injury. Sleep Science and Practice 2 (1), 2. https://doi.org/10.1186/s41606-018-0020-4.